One-dimensional electronic states at surfaces

2001 J. Phys.: Condens. Matter 13 11097

(http://iopscience.iop.org/0953-8984/13/49/301)

INSTITUTE OF PHYSICS PUBLISHING JOURNAL OF PHYSICS: CONDENSED MATTER

J. Phys.: Condens. Matter **13** (2001) 11097–11113 PII: S0953-8984(01)26229-8

One-dimensional electronic states at surfaces

F J Himpsel[1], K N Altmann[1], R Bennewitz[1,2], J N Crain[1], A Kirakosian[1], J-L Lin[1] and J L McChesney[1]

[1] Department of Physics, University of Wisconsin—Madison, 1150 University Avenue, Madison, WI 53706, USA
[2] Department of Physics and Astronomy, University of Basel, 4056 Basel, Switzerland

Received 25 June 2001
Published 10 December 2001
Online at stacks.iop.org/JPhysCM/13/11097

Abstract

One-dimensional electron systems can now be synthesized at stepped surfaces by self-assembly of atomic and molecular chains. A wide variety of adsorbate and substrate combinations provides opportunities for systematically tailoring electronic properties, such as the intra-chain and inter-chain coupling, the electron count, magnetic moment and the Coulomb interaction. Angle-resolved photoemission with synchrotron radiation is an ideal probe to reveal the complete set of quantum numbers for electrons at an ordered surface, i.e. energy, momentum parallel to the surface, spin and point group symmetry. Interesting electronic features are discussed, such as spin–charge separation in a Luttinger liquid, charge density waves, the Peierls gap, mixed dimensionality and one-dimensional quantum well states.

1. One-dimensional electrons

The properties of electrons become more and more exotic as one progresses from the three-dimensional world into lower dimensions. In a two-dimensional electron gas one observes surprising phenomena already, such as fractional charge and statistics for the fractional quantum Hall effect. The correlated motion of electrons and magnetic vortices generate such unusual phenomena [1]. Predictions for one-dimensional electrons are even more exotic. In a Luttinger liquid [2–12] the electron loses its identity and separates into two quasiparticles, a spinon that carries spin without charge, and a holon that carries the positive charge of a hole without its spin [12]. These two quasiparticles have different group velocities and run away from each other.

Figure 1 shows the spectral function of a one-dimensional Luttinger liquid, plotted versus energy and momentum. It describes the spectral weight observed in a photoemission experiment after taking out matrix element effects [7, 13]. These are predictions from extensive quantum Monte Carlo calculations, which are required to describe these many-body phenomena [6]. The spectral function can be decomposed into two peaks that change their energy $E = \hbar\omega$ linearly with the momentum $\boldsymbol{p} = \hbar\boldsymbol{k}$. These two peaks coincide at the

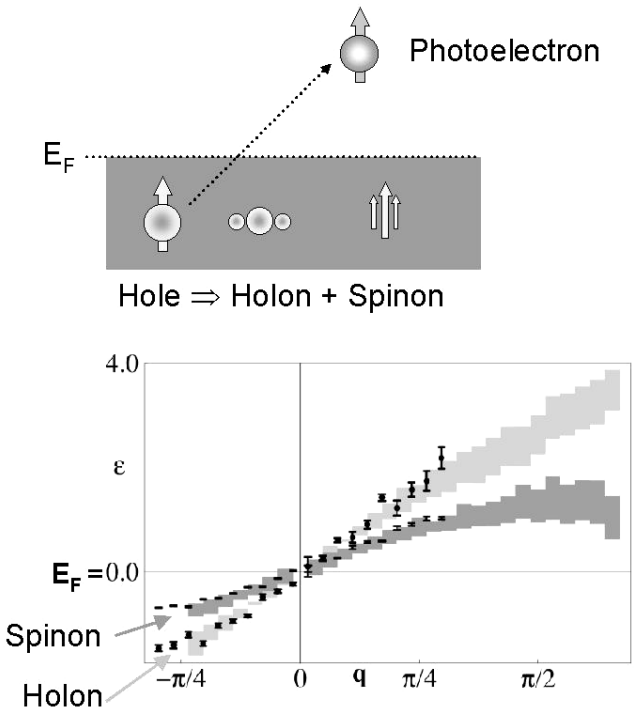

Figure 1. Spin–charge separation in a metallic Luttinger liquid, calculated from first principles. An ordinary energy band splits into two bands with different group velocities which intersect at the Fermi level. The spinon can be viewed as collective spin excitation, the holon as collective charge excitation. From [6].

Fermi level only, where the spinon and holon lines intersect. The slope $\mathrm{d}E/\mathrm{d}p = \mathrm{d}\omega/\mathrm{d}k$ gives the group velocity of the quasiparticles that correspond to peaks in the spectral function. The spinon has a larger group velocity than the holon by almost a factor of two. Note that the spinon and holon peaks in the spectral function overlap somewhat due to their finite width. That makes it easier to understand how spin and charge can be conserved when probing a holon or a spinon by photoemission, where a real electron with both spin and charge is ejected. When sitting on the spinon peak there is still a small contribution from the tail of the holon peak, which provides the charge required for the photoelectron. Likewise, the holon peak still contains a bit of spin character from the spinon tail.

The increasing amount of correlation between electrons in lower dimensions can be rationalized by a simple, classical picture where electrons behave like billiard balls (figure 2). They are forced into head-on collisions in one dimension because they cannot escape each other on a one-dimensional track. In quantum-mechanical terms, their wave packets have to penetrate each other at some point in time and thereby generate maximum overlap. In two and three dimensions such a situation is very improbable. The momenta of the electrons would have to be exactly opposite to each other and their positions would have to lie on the same line. There is an infinite number of other momenta available at the Fermi surface, where the most interesting electronic state reside. In one dimension, however, the Fermi 'surface' consists of two points with wavevectors $\pm k_F$. As a consequence, there is no such thing as a single electron in one dimension. When exciting it during the measurement process one necessarily generates a chain reaction that excites other electrons. The result is a collective excitation.

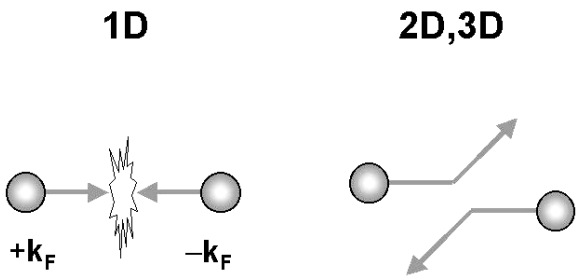

Figure 2. Intuitive picture rationalizing the increasing amount of correlations and many-body effects in one dimension. Two electrons from the two points $\pm k_F$ of the one-dimensional Fermi 'surface' collide head on, a situation that is highly unlikely in two and three dimensions where infinitely more combinations of momenta exist that avoid such a head-on collision.

Consequently, one may visualize a holon in a Luttinger liquid as a charge density wave and a spinon as a spin density wave.

Exotic phenomena, such as spin–charge separation, have mainly been discussed for metallic systems. They allow infinitesimally small excitations and are sensitive to tiny perturbations. For one-dimensional systems, however, the very existence of a metal is in question. A well known theorem by Peierls [14] argues that a one-dimensional chain of atoms is unstable to a pairing of the atoms, which creates an energy gap in the band structure at the Fermi level. The energy gained by lowering the occupied states at the bottom of the gap exceeds the strain energy that is necessary for the displacement. In fact, it has been difficult to find one-dimensional systems that are metallic. Fortunately, the Peierls theorem has its limitations, which allow for the existence of one-dimensional metals with exotic properties. One way out of the Peierls theorem is an atomic chain anchored to a rigid substrate, such as the metal chains on silicon discussed in the following. Thereby, the cost in strain energy becomes too high for pairing. The tightly bound carbon nanotubes appear to remain metallic as well, as long as their geometry allows a metallic band topology. Another loophole in Peierls' theorem is a band structure with more than one band, where the Fermi momentum is not located at the half-way point of the Brillouin zone [15].

Arrays of chains make it possible to study the interaction between two exotic electron liquids [10, 11]. For example, chain models have served as prototypes of complex, two-dimensional systems, such as high temperature superconductors with multiple CuO_2 layers in the unit cell [10]. The critical temperature T_c depends on the number of CuO_2 layers, suggesting that hopping between adjacent layers is a key to superconductivity. It has been disturbing that photoemission experiments have not resolved the inter-layer splitting expected from band calculations, but a spin–charge separated Luttinger liquid might offer an explanation. Calculations show that the non-Fermi-liquid nature of the states competes with inter-layer hopping and might be winning in that case [10]. Another topic of current interest is the spontaneous formation of stripes in such highly correlated materials [16], where metallic and insulating phases alternate over a period of a few nanometres. While these stripes fluctuate dynamically in most materials, they can be frozen in. That facilitates the study of the driving mechanism for such a spontaneous phase separation.

Magnetic chain structures exhibit several interesting excitations, such as the Haldane gap [17] in antiferromagnetic chains of integer spins. This gap separates the ground state, a non-magnetic singlet, from the lowest excitation, a spin 1 triplet. This gap disappears in higher dimensions where spin waves with arbitrarily low excitation energy exist. The Haldane gap lies

at the border of the energy scale currently accessible to photoelectron spectroscopy (>2 meV) and can be accessed at low temperature by inelastic neutron scattering. Ferromagnetism has been predicted for chains of non-magnetic atoms [18]. The density of states is strongly enhanced near one-dimensional van Hove singularities and can trigger a ferromagnetic phase transition via the Stoner criterion. There are many options for tailoring magnetic anisotropy at steps [19]. Steps create extra term in the magnetic anisotropy due to anisotropic strain combined with magnetostriction, anisotropic orbitals combined with spin–orbit interaction, shape anisotropy favouring magnetization parallel to long wires and magnetic dipole interaction favouring alternating spin orientation for adjacent wires.

In this article we will discuss the possibilities for using anisotropic surfaces to create new types of one-dimensional structure and for probing them with angle-resolved photoemission with synchrotron radiation. Section 2 shows that there are many ways to generate one-dimensional chains at surfaces, among them step arrays at semiconductors [20] and metals [21–25], decoration of steps [26–29] and chains of adsorbates [30–52]. Quite a few of these structures have been probed by photoemission or inverse photoemission. These techniques provide a complete picture of the occupied and unoccupied electronic states, i.e. holes and electrons [13]. Our emphasis will lie on semiconductor and insulator substrates [33–52], where the absolute band gap of the substrate prevents hybridization of chain states with three-dimensional states from the substrate and shorting of atomic wires by the substrate. That makes them an attractive option for atomic-scale electronics [53]. In particular, we will use low-dimensional structures induced by metals at a silicon surfaces [37–52] to illustrate the variety of interesting electronic phenomena encountered in one-dimensional systems. An example is the observation of a band splitting that has been suggested as an indication of spin–charge separation in a Luttinger liquid [46], but is likely to be a bonding–antibonding splitting of two coupled chains [47].

2. One-dimensional structures

The traditional approach to one-dimensional solids is based on three-dimensional crystals consisting of weakly coupled chains, for example rows of transition metal ions kept apart by a rigid lattice of counterions. They produce a large measurement volume for bulk-sensitive experiments, such as neutron scattering. However, the residual coupling between the chains is difficult to control, and the experimentalist is left to the mercy of Nature's quirks in forming crystalline structures. Polymers are more flexible towards tailoring the chain spacing by adding branches, but they do not order very well. More recently, the synthesis of highly-perfect nanowires, such as carbon nanotubes, has stimulated the investigation of individual objects with one-dimensional character. The capabilities of probing the electronic structure on an individual nanowire are still rather rudimentary, however. It is very difficult to attach leads to a single nanowire that connect it to the macroscopic world. Fabricating contacts by conventional lithography introduces surface contamination that influences the electronic structure of the nanowire. It has been tempting to use several decades of experience with surface science techniques for obtaining a clean and well ordered array of chains at a surface. Locking the chains to a crystalline substrate as a superlattice makes it possible to control their spacing with atomic precision. A well-suited analysis method is photoemission with ultraviolet radiation. It is surface sensitive and provides the full complement of quantum numbers for electrons in a periodic medium, such as a single crystal surface [13]. The energy, the momentum parallel to the surface, and the spin are obtained by measuring these quantities for the emitted electrons and using conservation laws. The point group symmetry follows from the polarization dependence via optical dipole selection rules.

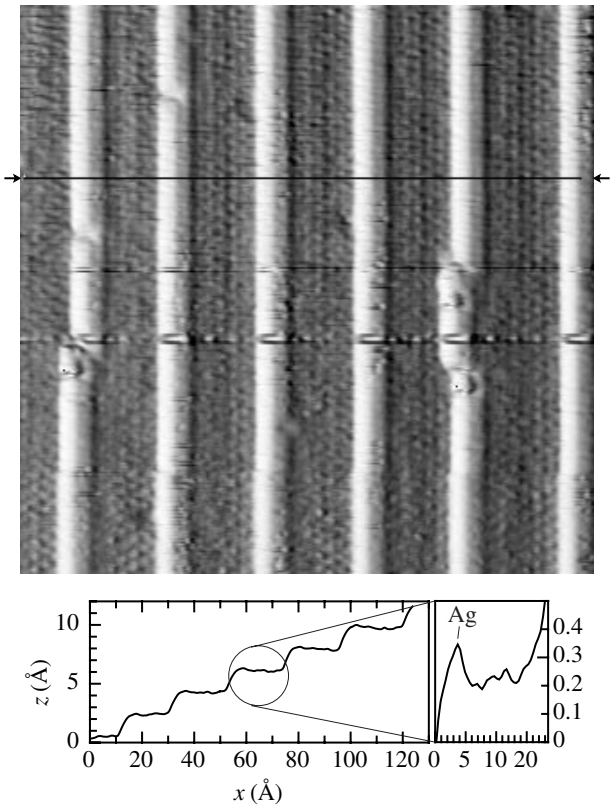

Figure 3. Decoration of step edges for Ag on Pt(997), a highly-stepped Pt(111) surface. The x-derivative of the STM topography is shown (top), which produces white lines at the step edges (uphill to the right). The presence of a row of Ag atoms at the step edge is seen in the constant current line scan at the bottom as an extra peak at the step edge. From [27].

Stepped surfaces with a slight miscut from a crystallographic plane form ideal templates for atomic chains. Figure 3 shows how step edges can be decorated by evaporating metal atoms [26]. The dominant white lines in this STM image are the step edges of a Pt(997) surface, imaged in a derivative mode. To their right are the Ag atom chains, which can be seen more clearly as extra peaks in the line scan below. Pseudomorphic chains of atoms are difficult to image in the topographic STM mode since there is no structural difference discriminating them from the substrate. Spectroscopic imaging via resonant tunnelling makes such atoms more visible [26]. The method of step decoration has turned out to be rather flexible, with at least two independent control parameters. The miscut angle determines the step spacing and thus the coupling between the chains. The metal coverage determines the number of atomic rows that are attached to the step edges, and thereby the number of independent wavefunctions forming conduction channels. Particularly interesting is the limit of a single atom row attached to a step edge, as shown in figure 3 [27]. For varying the coupling along the chains one can choose metal atoms with different sizes. Atoms with a magnetic moment will generate additional magnetic couplings [29].

The most perfect step arrays have been fabricated at surfaces with a large-scale reconstruction, such as Si(111)7 $\times$ 7 [20] and Au(111) [21]. In that case the formation of a kink (the native defect of a step array) requires adding many rows of atoms and generates

a kinetic barrier. For example, a kink at the Si(111)7 × 7 surface requires the addition of 14 atomic rows (seven rows two layers deep). Kink densities as low as one in 20 000 edge atoms have been achieved. In addition, the terrace width becomes quantized in units of the reconstructed surface. By going to a dense step array with a single such quantum as terrace width one is able to produce an array with uniform step spacing.

Even flat surfaces can serve as templates for arrays of one-dimensional chain structures. An intrinsic anisotropy may introduce a preferred growth direction, such as for the (110) surface of cubic structures. The (110) of the fcc lattice, in particular, exhibits deep grooves in the directions which can serve as sites for adsorption and rapid diffusion.

Isotropic surfaces with three- or four-fold symmetry are not immune to anisotropy, either. Spontaneous symmetry breaking may create several equivalent domains of oriented chains. Below we will discuss chain structures on Si(111) which are formed with three domain orientations on the flat surface. A small miscut of typically 1° selects one of the domains exclusively, as long as it is chosen such that the step edges are parallel to the chains of the surface reconstruction.

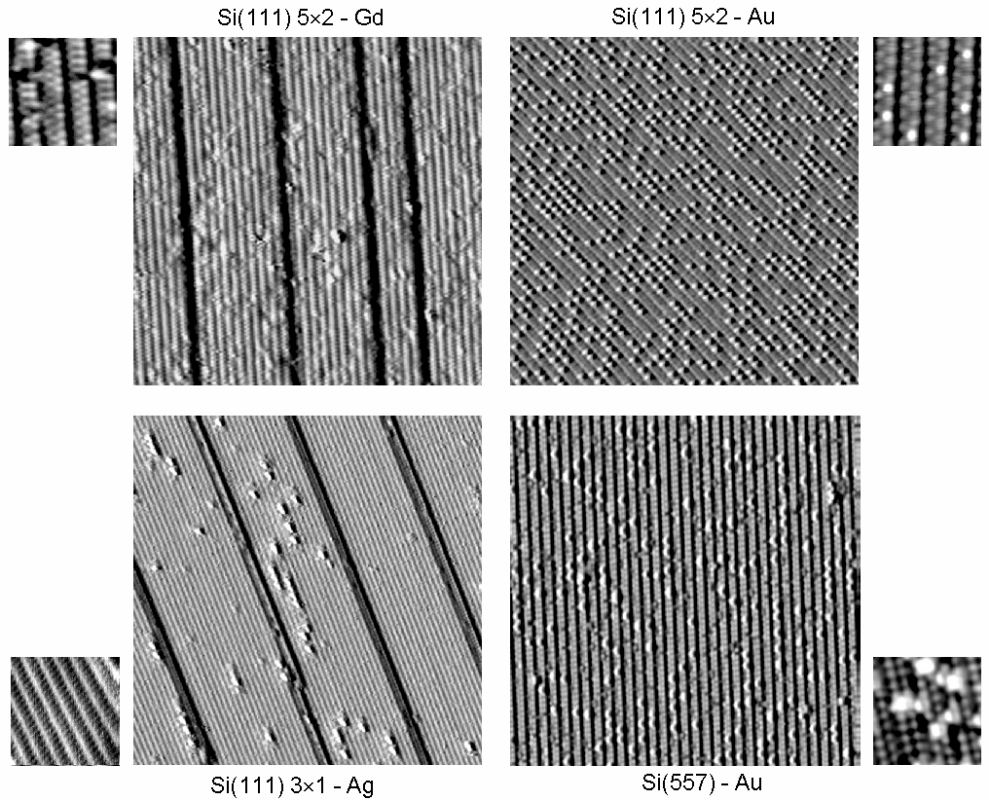

Figure 4. Chain structures of Au, Ag, and Gd on silicon, showing the variety of one-dimensional chain structures that metals form on Si(111) at low coverage. The overview panels (60 × 60 nm^2) show the x-derivative of the topography, which produces dark lines at the step edges (uphill to the left). The close-up panels (7 × 7 nm^2) show the topography itself. Compare [47] and [48] for Au, [56] for Ag and Gd.

Chain structures induced on a semiconductor surface by metal atoms are shown in figure 4. Some are formed on flat Si(111) and stabilized as single domain with a 1° miscut towards $[\bar{1}\bar{1}2]$;

others occur on Si(557), a highly-stepped version of Si(111) with a terrace width of $5\frac{2}{3}$ atom rows. These STM images clearly demonstrate a long-range reconstruction consisting of one-dimensional chains. The lattice period along the chain is doubled, possibly due to Si adatoms on every other lattice site. Adatoms tie up three broken bonds and trade them in for one. For clean Si(111)7 × 7 they provide the primary mechanism for lowering the surface energy. Adjacent chains seem to lack phase correlation since about half of the chains are arranged in a 2×2 zig-zag pattern, and the other half in a $c(4 \times 2)$ ladder structure, as seen in the inset. Such disorder leads to faint streaks at the half-order positions in diffraction experiments [54], as well as in the Fourier transform of the STM images. Such uncorrelated chains have been found for the honeycomb chain structure of Si(111)4 × 2–In, too [38]. The lack of correlation between adjacent chains suggests weak inter-chain coupling and a truly one-dimensional electronic structure.

There are several other techniques for producing arrays of nanowires at surfaces. However, we restrict ourselves to systems where the electronic structure has been determined by angle-resolved photoemission and inverse photoemission.

3. Metal surfaces

At stepped surfaces of clean metals one might expect a slight change in the electronic structure for the step edge atoms. Their coordination is reduced, which leads to a narrowing of the valence bands and a core level shift, using basic tight binding and band filling arguments. Such level shifts are relatively small, however, and remain close to the limit of detection imposed by the intrinsic lifetime broadening for core levels and for the more localized, d-like valence bands of transition and noble metals.

In order to obtain an appreciable effect it is useful to choose the rather delocalized s, p-like valence states close to the Fermi level in simple metals and noble metals. A classic case has been the Cu(111) surface state near the centre Γ of the surface Brillouin zone. It has produced standing waves that become visible by STM when the wavefunction is confined to a quantum corral of adsorbed atoms [55] or to a terrace between steps [24, 25]. It is interesting to view the wavefunction of such a state on a step lattice from two extremes and see how the transition between them occurs [23]. For widely-separated steps one has the wavefunction of a flat Cu(111) surface with extra boundary conditions at the steps. They give rise to a lateral quantization by forming standing waves between the steps. These are seen by STM [27, 55]. For closely-spaced steps we can think of the surface as a high-index plane and use a wavefunction that is tied to the average (optical) surface, not to the (111) terraces. The reciprocal lattice vectors of the step lattice $g_n = n^2\pi/d$ transfer discrete k-vectors to the wavefunction, which can be seen as a back-folding of the bands perpendicular to the steps (d = step spacing). Most STM work has been restricted to the first extreme, i.e. rather flat surfaces, whereas most photoemission work has dealt with the second case, i.e. rather dense step arrays. These choices are connected with the fact that STM operates in real space and wants to sample large spatial features to obtain many data points, whereas photoemission operates in k-space and wants a large angular range for many k-points. This gap has been bridged, and a transition has been found between the two limits at a miscut angle of about 7° [23]. Lateral quantum well states have been observed not only by STM [24], but also by photoemission on highly-perfect Au(111) step lattices [25].

The same s, p-like surface state can be used to explore the electronic states at decorated step edges, as shown in figure 5 [28]. Cu wets the surface and the step edges of W(110) and Mo(110) due to its low surface energy. On the highly-stepped W(331) surface with six atomic rows per terrace one can compare a two-dimensional Cu film at monolayer coverage with an array of

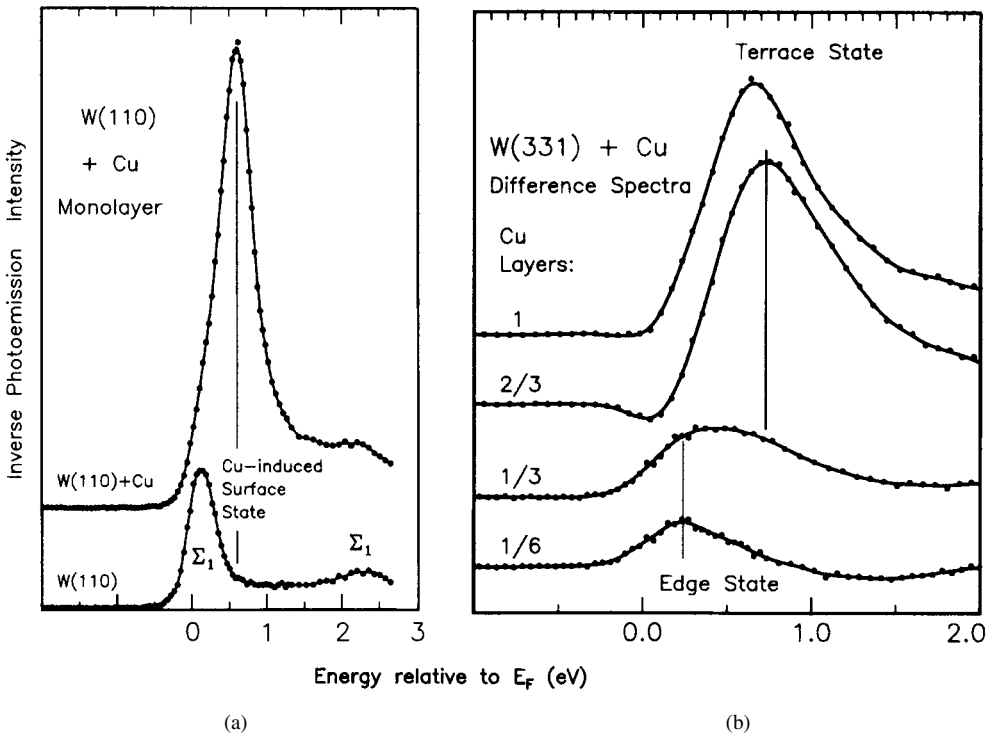

Figure 5. Two- and one-dimensional states of Cu on stepped W(110), probed by angle-resolved inverse photoemission. From [28]. (a) Two-dimensional surface state of Cu in the s, p gap on W(110). (b) One-dimensional state for a single row of Cu atoms adsorbed at the edge of each W terrace on W(331), a highly-stepped W(110) surface.

single Cu chains at 1/6 of a monolayer coverage. The first Cu layer occupies the lattice sites of bcc W(110) and Mo(110) and thereby forms a slightly-stretched, hexagonal lattice resembling the hexagonal surface of fcc Cu(111). The Cu(111) surface states shifts from slightly below the Fermi level to slightly above and can be observed by inverse photoemission [28]. Its rapidly-increasing cross section at low photon energies (<10 eV) reveals that the feature depicted in the difference spectra in figure 5 is as the analogue to the Cu(111) surface state [13]. When reducing the coverage down from a monolayer in figure 5 one observes no change in the energy of the surface state until the single row limit of 1/6 monolayers is reached.

A variety of anisotropic adsorbate structures have been investigated that form chains [31, 32]. Early work on thallium on Cu(100) found evidence for thallium chains at sub-monolayer coverage with one-dimensional dispersion and the possibility of a Peierls gap [32]. Atoms form chainlike structures on anisotropic metal surfaces, such as such as H on Ni(110) and O on Cu(110) [31]. The E versus k band dispersion is one dimensional for the adsorbate orbitals. One may view such systems as insulating 'antiwires' on a metallic substrate.

A general problem with one-dimensional structures on metals is the hybridization of the chain orbitals with the bulk states. In general, two electronic states will hybridize if they have the same energy E and momentum $\boldsymbol{p} = \hbar\boldsymbol{k}$, plus the same symmetry. Truly two-dimensional states need to be located in a symmetry gap of the projected bulk bands. All bulk states along a 'rod' with variable wavevector perpendicular to the surface $k^{\perp}$ can interfere, as long as their parallel wavevector $k^{\parallel}$ is the same. This holds because the direction perpendicular to the

surface is not translation invariant and, thus, does not conserve $k^{\perp}$. At a surface step the in-plane translation invariance is broken in the direction perpendicular to the step. An additional projection of all bulk $\boldsymbol{k}$-vectors in that direction is called for. Such doubly-projected bulk bands leave practically no room for a gap in a metal. That effectively closes the window of opportunity for a gap in the doubly-projected bulk bands. With a step array the situation is slightly different, because the surface remains periodic. However, there is a large number of reciprocal lattice vectors of the step superlattice $g_n = n2\pi/d$ that can transfer momentum perpendicular to the steps. Effectively, one has to back-fold the bands N times in the plane of the surface if N is the number of atomic rows per terrace. This problem can be overcome by an absolute gap on a semiconductor or insulator.

4. Semiconductor surfaces

Clean semiconductor surfaces display a rich variety of chain structures with one-dimensional electronic states. A well studied case is the metastable, cleaved Si(111)2 $\times$ 1 surface which rearranges itself into π-bonded chains in order to make up for the broken bonds by additional π-bonds [33, 34]. Its electronic structure is characterized by a pair of π and π^* bands that have one-dimensional character near the Brillouin zone boundary, where they stay clear of the projected bulk bands. The interaction is large along the chains as evidenced by the band width of 0.8 eV. This is to be compared to a band width of 0.1 eV perpendicular to the chains. There is a significant gap of 0.5 eV between the occupied π band and the unoccupied π^* band that can be traced to the presence of two inequivalent atoms in the chain. In fact, the chain is highly tilted with one atom moving away from the surface and becoming negatively-charged, and the other moving in and acquiring positive charge. There is no dimerization along the chain and, therefore, no Peierls distortion. The analogous π-bonded chain structure carbon in polyacetylene, on the other hand, dimerizes into alternating single and triple bonds.

Adsorbed alkali atoms arrange themselves into finite chain segments on GaAs(110) and similar III–V surfaces [35], which by itself has already chain character. These chains behave as insulating in scanning tunnelling spectroscopy and photoemission, despite the fact that increasing the electron count per unit cell by one should convert a semiconducting surface with filled bands (paired electrons) into one with a half-filled band (unpaired electron). The likely culprit in this case is a Mott–Hubbard transition from a metal to a semiconductor, where a band holding both spin orientations splits into two bands holding only one spin each. It happens when the extra Coulomb energy U for a second electron on the same site becomes larger than the band width W, which is determined by the coupling (overlap) along the chain. Theoretical estimates of the Coulomb energy U for alkali metals on semiconductors support this explanation [36]. Semiconductors have a tendency towards such correlation effects due to their localized broken bonds, which reduce the hopping rate along the chain. For a long time it has been difficult to produce metallic surfaces on semiconductors, even in cases where an odd electron count in the unit cell would indicate a metallic band structure.

In recent years, several metallic chain structures have been found on semiconductor surfaces [38–50]. They raise hopes for the discovery of interesting new phenomena in one-dimensional electron liquids. The Si(111) surface has been particularly useful as a substrate, not only for achieving metallic character, but also for obtaining particularly straight and regular step arrays (see section 2). The two Au structures in figure 4 are metallic [43, 44, 46–48]; the Ag and Gd structures are currently under investigation by photoemission [56]. Another metallic chain structure is formed by In on Si(111) [38, 39]. Four atomic rows of In form a ribbon-like honeycomb chain structure, which has suggested [37] as a rather widespread feature of metal

adsorbates on Si(111). In the following, we will discuss the characteristic of the three metallic surfaces. It turns out that each of them exhibits a peculiar electronic feature.

Gold adsorbed on stepped Si(111) surfaces forms two distinct, one-dimensional structures, i.e. the highly-stepped Si(557)–Au [46–48] and flat Si(111)5 × 2–Au [43, 44, 48]. Both exhibit chains of atoms along the $[\bar{1}10]$ direction, as shown in figure 4. In both cases the unit cell contains five atomic rows of the unreconstructed surface. The Si(557)–Au surface contains an additional double-step per unit cell. Although the two Si–Au structures have common features, some of the basic electronic characteristics are quite different, such as the Au content and the electron count. Si(557)–Au contains 0.2 monolayers of Au, which is equivalent to a single Au row per unit cell [45–48]. Si(111)5 × 2–Au contains twice as much Au, i.e. 0.4 monolayers or the equivalent of two Au rows per unit cell [41, 43, 44, 48]. For determining the number of unpaired electrons per unit cell we start out with the unreconstructed Si(111)5 × 1 and Si(557) surfaces and add the Au atoms later. Extra silicon atoms incorporated during the reconstruction do not affect the parity of the electron count because they contain four electrons each. The unit cell of Si(111)5 × 1 contains five surface atoms with a single broken bond each. Si(557)1 × 1 has five such atoms on the terrace, plus an extra atom with two broken bonds at the step edge, bringing the number up to seven. Next, we add Au atoms with an unpaired s electron each. With two Au electrons for Si(111)5 × 1–Au and one Au electron for Si(557)–Au we obtain a total of seven electrons for Si(111)5 × 1–Au and eight electrons for Si(557)1 × 1–Au. In a simple band model with two spin-paired electrons per band one would expect Si(111)–Au to be metallic and Si(557)–Au to be semiconducting.

The experimental band dispersions for the two Si–Au surfaces are shown in figure 6. They demonstrate clearly that the electronic structure can be tailored by choosing the step density and the Au coverage. The Si(111)–Au bands appear to be semiconducting with a 0.3 eV gap below the Fermi level E_F, and the Si(557)–Au bands are metallic. This seems to be at odds with the expectations from the electron count. This contradiction is resolved in the following by invoking period doubling for the gap for Si(111)–Au and by observing that two bands cross the Fermi level for Si(557)–Au, each of them contributing one electron. Furthermore, there exist additional, truly-metallic bands for Si(111)–Au that are barely visible in figure 6 but appear in the second Brillouin zone in figure 7.

The shape of the bands in figure 6 is similar for the two chain structures, suggesting a common origin related to a particular type of chain. In both cases we observe a dominant band that is about 1.0 eV wide and extends from a minimum at the zone boundary $\pm\pi/a = \pm 0.82$ Å^{-1} to the point of half filling at $\pm\pi/2a$. There are two differences: the Si(557)–Au band splits into a pair, and the Si(111)5 × 2–Au band is shifted down by 0.3 eV, leaving a gap at the Fermi level. This is not a true gap since it is filled in by a set of additional, metallic bands in the second Brillouin zone beyond $\pm\pi/a$. The slope of the bands in figure 6 gives a Fermi velocity $v_F = \hbar^{-1}\,\mathrm{d}E/\mathrm{d}k = -1.0 \times 10^6$ m s^{-1}. For comparison, the value for bulk Au is $v_F = +1.4 \times 10^6$ m s^{-1}. The band topology is quite different, i.e. hole-like for Au chains on Si versus electron-like for bulk Au.

For Si(557)–Au, the observed band splitting at E_F rules out the spinon–holon splitting suggested as its origin initially [46]. Spinon and holon bands have to converge at E_F, as shown in figure 1 [6]. Furthermore, having just a single band cross the Fermi level would not be compatible with the even electron count. The same argument rules out other splitting mechanisms for a single band, such as a spin splitting. A natural interpretation of the splitting is a closely-spaced doublet of ordinary bands crossing E_F. It explains why we have a metallic surface despite an even electron count per unit cell. Each of the half-filled bands contributes one electron. Two nearly-degenerate energy bands suggest two nearly-identical orbitals within the unit cell that generate bonding/antibonding combinations, corresponding

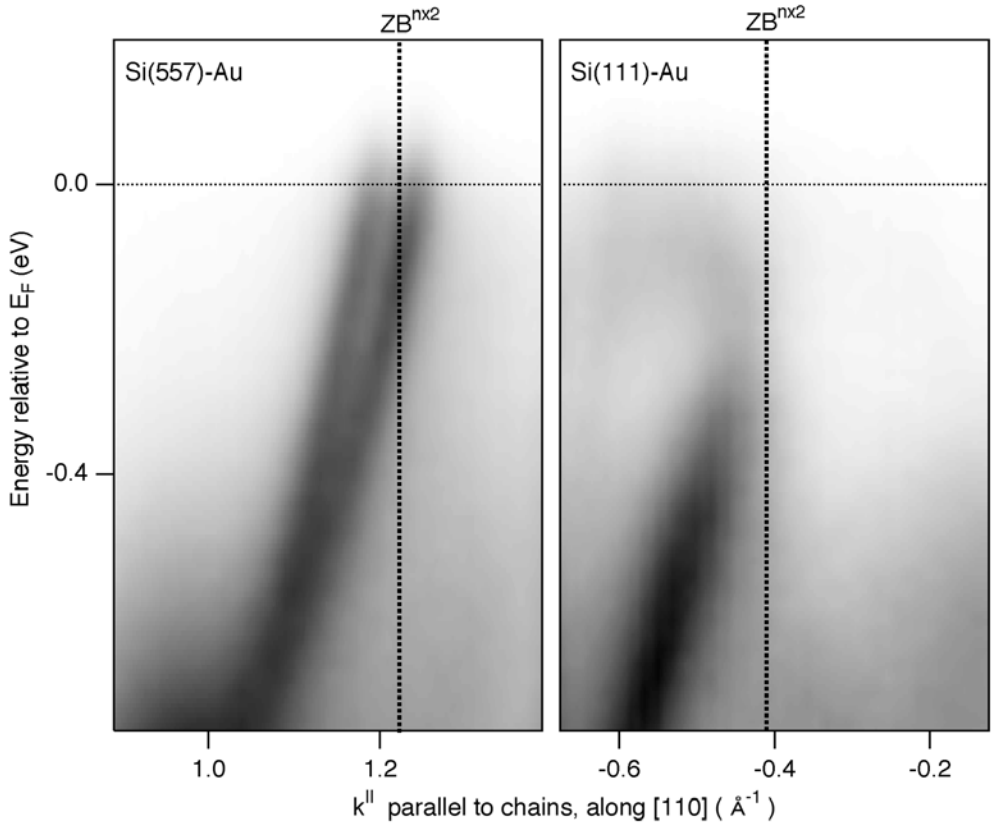

Figure 6. Modification of the band structure by changing the electron count. Surprisingly, the Si(557)–Au surface with an even electron count is metallic, and the Si(111)–Au surface with an odd electron count exhibits a pseudo-gap. High photoemission intensity is shown dark in these experimental bands, obtained by energy and angle multidetection. Compare [47] and [48].

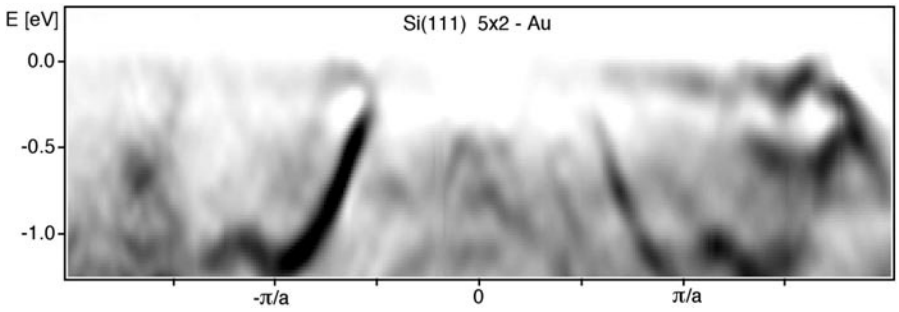

Figure 7. Energy bands of Si(111)–Au over a wider $\boldsymbol{k}$-range. Extra, metallic bands show up in the second Brillouin zone. The right–left asymmetry is due to the polarization vector $\boldsymbol{A}$ of the photon in the photoemission matrix element. High photoemission intensity is shown dark. Compare [48].

to even/odd superpositions of the two wavefunctions. For example, the two orbitals could originate from two chains in the unit cell or from two orbitals located on a single chain, such as the two broken bonds at the step edge or a set of in-plane, $p_{x,y}$ orbitals connecting atoms in

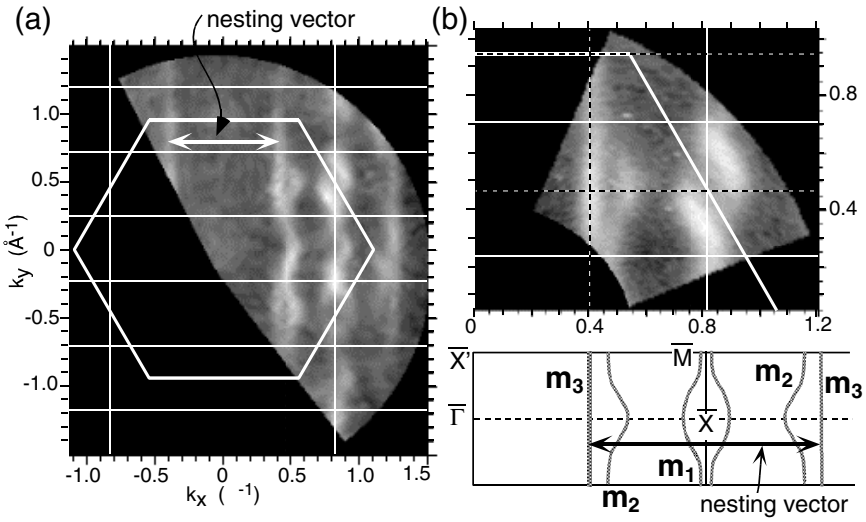

Figure 8. Fermi surface for Si(111)4 × 1–In, mapped by angle-resolved photoemission. A Peierls transition at low temperature is related to the band m_3, which has a one-dimensional Fermi surface at the point of half-filling. High photoemission intensity is shown light. From [38].

a zig-zag chain. In fact, the STM image of Si(557)–Au in figure 4 does reveal two chains per unit cell. However, the atomic structure of this surface is still under investigation [49, 50], and it not clear yet whether the two chains observed by STM are related to the two sets of orbitals seen in photoemission.

For Si(111)5 × 2–Au there is a pseudo-gap at the location in $\boldsymbol{k}$-space where one would expect a Peierls gap, but its magnitude of about 0.3 eV is far greater than what one can expect from a Peierls distortion. Such a large gap can be rationalized by the natural tendency of the Si(111) surface to create adatom structures with a doubled unit cell. The lattice distortion is much larger than for a Peierls distortion in this case, because every other atom is actually missing, not only displaced. Consequently, the period doubling remains up to temperatures well above room temperature, whereas the Peierls transition reported for Si(111)4 × 1–In occurs below room temperature [38].

The Si(111)4 × 1–In surface has been studied both by angle-resolved photoemission [38] and by first principles band calculations [15]. It contains about a monolayer of In, corresponding to four atomic rows of In arranged in a honeycomb chain [15, 37]. The corresponding four bands are observed in photoemission [38]. Three of them intersect the Fermi level. This surface exhibits a Peierls-like phase transition below room temperature, where the period along the chain is doubled and the bands crossing the Fermi level open up a gap. The origin of this phase transition can be traced to one of the bands, as shown in figure 8. This figure displays the Fermi surfaces of the three metallic bands. For a two-dimensional surface state the Fermi surface is a one-dimensional curve. If the surface has one-dimensional chain character this curve becomes a straight line parallel to the chain. The wavevector perpendicular to the chain ceases being a quantum number and the energy surface cannot depend on it.

Constant energy surfaces, such as shown in figures 8 and 9, focus on the part of the energy bands that is relevant to electronic phase transitions and transport properties [38, 44, 57]. The Fermi surface, in particular, plays a dominant role in determining electronic phenomena. All the states relevant to an electronic phase transition are located within energies that are accessible

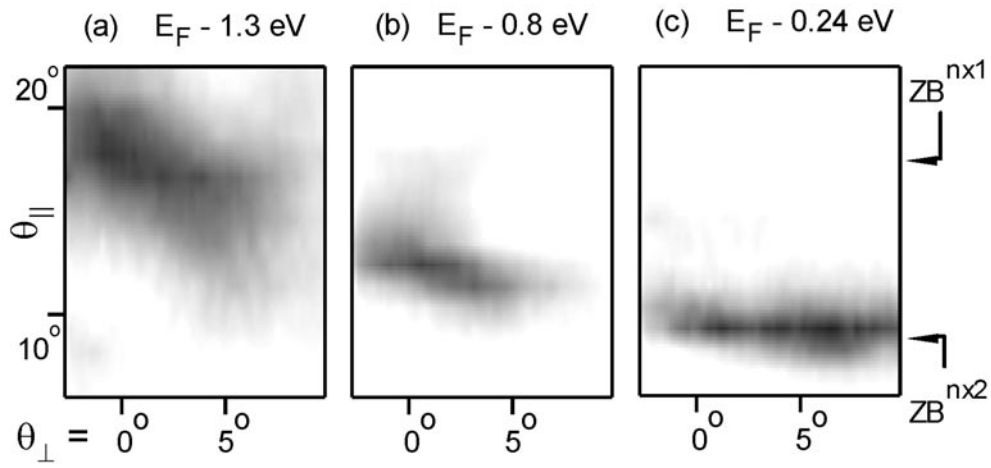

Figure 9. Transition from a two-dimensional to a one-dimensional energy surface for same band, observed in Si(111)–Au. The horizontal line for the top of the band is located in the same region of $\boldsymbol{k}$-space as the vertical line for the $\boldsymbol{m}_3$ band in figure 8. High photoemission intensity is shown dark. From [44].

to thermal excitations at the critical temperature T_c, and the gap E_g is comparable to those energies. In mean-field theory, such as in the BCS theory of superconductivity, the relation between gap and critical temperature is $E_g \approx 3.5\ k_B T_c$ (k_B = Boltzmann constant). This value is nearly the same as the width of the Fermi Dirac function at T_c, when defined as the full width at half maximum of its derivative. The numerical factor 3.5 increases for strongly-coupled systems, such as high temperature superconductors, and reaches about 10 for the Si(111)4 × 1–In surface. The state $\boldsymbol{m}_3$ in figure 9 has two properties that make it a prime candidate for triggering the Peierls transition. It has a straight, one-dimensional Fermi surface, and it is located half-way to the zone boundary along the chain. That is the point in $\boldsymbol{k}$-space where the Peierls transition opens up a gap and lowers the energy of the states just below the Fermi level. The analogous point for the Au chains on silicon is labelled $\mathrm{ZB}^{n\times 2}$ in figure 8.

Si(111)5 × 2–Au exhibits a second unusual feature, apart from the large pseudo-gap. A look at its constant energy surfaces in figure 9 (analogous to those for Si(111)4×2–In in figure 8) reveals a surprising change in dimensionality when going from the top of the band towards the bottom. At the bottom one finds a diagonal energy contour which indicates a two-dimensional band dispersion (both parallel and perpendicular to the chains). The tilt of the energy contour vanishes gradually towards the top of the band, where we have a horizontal, one-dimensional contour. The wavefunction corresponding to such a band must be quite unusual. At the top of the band it appears to be localized to a chain; at the bottom it extends out to neighbouring chains. That would be contrary to the expectation that states at higher energies are more delocalized. It turns out that such a band topology is not at odds with basic band theory. A simple band model can be constructed that reproduces the observed band topology [44, 58]. This is accomplished by a tight binding Hamiltonian that contains not only a coupling t_1 along the chains and a perpendicular coupling t_2, but also a diagonal coupling t_3 [58]. Essentially, t_2 and t_3 are able to compensate each other at a particular $k^{\|}$-point and eliminate the dispersion perpendicular to the chains at that point. Such behaviour can be explained intuitively by a mechanism that de-couples the chains at a particular $k^{\|}$-point by placing a node of the wavefunction on the atoms that couple the chains [44].

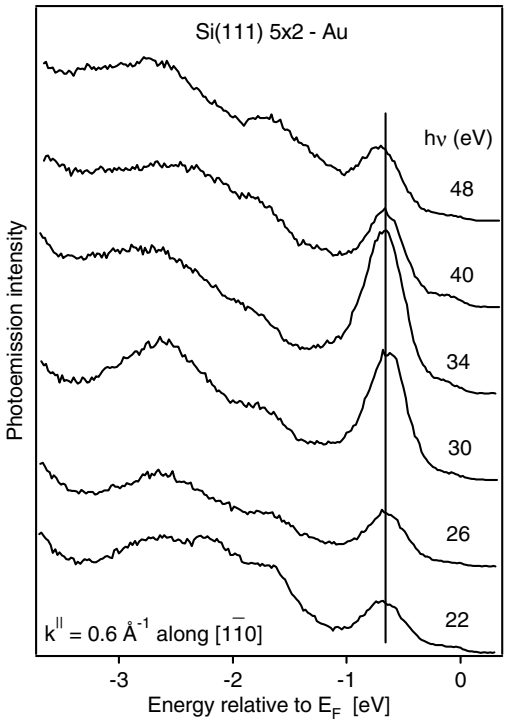

Figure 10. Maximizing the cross section of surface states relative to the bulk bands by tuning the photon energy at a synchrotron. For surface states on Si(111) the optimum photon energy lies near 34 eV. Compare [48].

5. Benefits of synchrotron radiation

Synchrotron radiation provides two key features that set it apart from a resonance lamp as a source of ultraviolet light, that is tunability and polarization.

Tuning the photon energy makes it possible to separate two- and one-dimensional surface states from three-dimensional bulk states of the substrate. By varying the photon energy one varies the component of k perpendicular to the surface [13]. Bulk states change their binding energy, whereas surface states are not affected since the perpendicular momentum is not one of their quantum numbers. Only the intensity of the surface states changes due to the photon energy dependence of the matrix element $\langle\psi_f|\boldsymbol{A}\boldsymbol{p}|\psi_i\rangle$ for photoemission ($\boldsymbol{A}$ is the vector potential of the photon, $\boldsymbol{p}$ the momentum operator and ψ_f and ψ_i the final and initial state wavefunctions). A combination of these two effects was used to bring out the surface states on Si(111) in figures 6, 7 and 9. As shown in figure 10, the surface states are strongest and farthest away from the bulk states at a photon energy $h\nu \approx 34$ eV. The He I resonance line generally produces much weaker features for surface states on Si(111). Synchrotron radiation can also be tuned to the Cooper minima in the cross section of the substrate, in order to bring out the weak signal from adsorbed atom chains [29].

The polarization of synchrotron radiation has also a strong effect on the intensity of surface states via the $\boldsymbol{A}$-vector in the matrix element. It can be used to determine symmetry properties of the states, such as even or odd reflection symmetry with respect to a mirror plane [13]. Even when there is no strict symmetry selection rule, the intensity variations can be very large and may be used to distinguish nearby surface states with different Wavefunctions. Figure 7 shows

that the intensities of the bands in opposite $\boldsymbol{k}$-directions are quite different from each other. The reason is a different orientation of the $\boldsymbol{A}$-vector. Positive $\boldsymbol{k}$ have a much larger component of $\boldsymbol{A}$ perpendicular to the surface for this particular configuration. The sample rotates, and the electron analyser is fixed at an angle of 50° from the incoming photons in the plane of the $\boldsymbol{A}$-vector and the surface normal.

6. Summary and outlook

The few examples given in this overview illustrate the variety of one-dimensional structures that can be obtained at anisotropic surfaces. A particularly flexible method is the decoration of stepped surfaces by adsorbed metal atoms. Real space information from STM is combined with reciprocal space data from photoemission. Angle-resolved photoemission and inverse photoemission are well matched to these systems and make it possible to measure their complete electronic structure. With state-of-the-art multidetection one can directly obtain the spectral function from the intensity $I(E, k_x)$, as shown in figures 6 and 7, and the Fermi surface from $I(k_x, k_y)$, as shown in figures 8 and 9. Synchrotron radiation as a tunable and polarized light source can be adjusted to the optimum cross section for enhancing the signal from sub-monolayer chains.

It is encouraging to see that a metallic ground state can be obtained in one-dimensional structures, such as for Si(557)–Au. Apparently, the anchoring of the chains to a rigid step lattice counteracts the tendency towards a metal–insulator transition via Peierls distortion. The variety of the observed electronic features illustrates the potential for tailoring the electronic structure of one-dimensional chains and ladders at surfaces. Several parameters are available for steering a surface towards specific sections of the phase diagram of one-dimensional electrons, such as charge density waves or exotic, non-Fermi liquids. The electron count can be varied by the metal coverage, the coupling between the chains by the step density, the coupling along the chain by the size of the adsorbed atoms and even the spin structure might be controllable by using magnetic atoms. Even though initial suggestions of spin–charge separation in such structures have not withstood closer scrutiny, it is quite possible that a chain structure with the coupling parameters appropriate for a Luttinger liquid can be designed.

It is interesting to note that the stripes observed in high temperature superconductors and other correlated electron systems [16] have widths quite comparable to the chain structures shown here. A well defined, static structure of alternating metallic and insulating stripes on vicinal Si(111) could become an excellent test case for testing theoretical models of stripes.

Before embarking on an ambitious program of tailoring one-dimensional solids we will need to understand the wavefunctions underlying their interesting features. First of all, that requires a structure determination coupled with a band structure calculation. That will be a challenge for both experiment and theory considering these large, highly-reconstructed unit cells.

Acknowledgments

Stimulating discussions with S C Erwin are acknowledged. This work was supported by the NSF under Award Nos DMR-9815416 and DMR-0079983. This work is based upon research conducted at the Synchrotron Radiation Center, University of Wisconsin—Madison, which is supported by the NSF under award No DMR-0084402.

References

[1] Stormer H L 1998 *Rev. Mod. Phys.* **71** 875
Laughlin R B 1998 *Rev. Mod. Phys.* **71** 863

Jain J K 2000 *Phys. Today* April 39
[2] Luttinger J M 1963 *J. Math. Phys.* **4** 1154
[3] Meden V and Schönhammer K 1992 *Phys. Rev.* B **46** 15 753
[4] Voit J 1995 *Rep. Prog. Phys.* **18** 997
[5] Shannon N and Joynt R 1996 *J. Phys.: Condens. Matter* **8** 10 493
[6] Zacher M G, Arrigoni E, Hanke W and Schrieffer J R 1998 *Phys. Rev.* B **57** 6370
[7] Grioni M, Vobornik I, Zwick F and Margaritondo G 1999 *J. Electron Spectrosc.* **100** 313
[8] Denlinger J D, Gweon G-H, Allen J W, Olson C G, Marcus J, Schlenker C and Hsu L-S 1999 *Phys. Rev. Lett.* **82** 2540
For an alternative view see Xue J, Duda L-C, Smith K E, Fedorov A V, Johnson P D, Hulbert S L, McCarroll W and Greenblatt M 1999 *Phys. Rev. Lett.* **83** 1235
[9] Kim C, Matsuura A Y, Shen Z-X, Motoyama N, Eisaki H, Uchida S, Tohyama T and Maekawa S 1996 *Phys. Rev. Lett.* **77** 4054
Fujisawa H, Tokoya T, Takahashi T, Miyasaka S, Kibune M and Takagi H 1999 *Phys. Rev.* B **59** 7358
[10] Chakravarty S, Sudbo A, Anderson P W and Strong S 1993 *Science* **261** 337
Clarke D G, Strong S P and Anderson P W 1994 *Phys. Rev. Lett.* **72** 3218
[11] Shannon N, Li Y and d'Ambrumenil N 1997 *Phys. Rev.* B **55** 12 963 and references therein
[12] The reason for the positive charge of the holon is not peculiar to a one-dimensional solid. It is simply related to the fact that one cannot probe the energy and momentum of an electron in a solid without ejecting it, for example as photoelectron in a photoemission experiment. That leaves the solid in a positively charged, excited state. In general, an occupied electronic state corresponds to an excited solid with a hole and an unoccupied state to an excited solid with an extra electron. An unoccupied state can be probed with inverse photoemission by injecting an electron.
[13] For a review on angle-resolved photoemission see Himpsel F J 1983 *Adv. Phys.* **32** 1
For a review of inverse photoemission from semiconductors see Himpsel F J 1990 *Surf. Sci. Rep.* **12** 1
[14] Peierls R F 1955 *Quantum Theory of Solids* (Oxford: Clarendon) p 108
[15] Erwin S C to be published
[16] Tranquada J M *et al* 1997 *Phys. Rev. Lett.* **78** 338
Emery V J and Kivelson S A 1995 *Nature* **374** 434
[17] Haldane F D M 1983 *Phys. Rev. Lett.* **50** 1153
[18] Zabala N, Puska M J and Nieminen R M 1998 *Phys. Rev. Lett.* **80** 3336
[19] Berger A, Linke U and Oepen H P 1992 *Phys. Rev. Lett.* **68** 839
Chen J and Erskine J L 1992 *Phys. Rev. Lett.* **68** 1212
Hyman R A, Zangwill A and Stiles M D 1998 *Phys. Rev.* B **58** 9276
Elmers H J, Hauschild J, Höche H and Gradmann U 1994 *Phys. Rev. Lett.* **73** 898
Kawakami R K, Bowen M O, Choi H J, Escorcia-Aparicio E J and Qiu Z Q 1998 *Phys. Rev.* B **58** R5924
Dorantes-Dávila J and Pastor G M 1998 *Phys. Rev. Lett.* **81** 208
Bode M, Pietzsch O, Kubetzka A, Heinze S and Wiesendanger R 2001 *Phys. Rev. Lett.* **86** 2142
For a review of magnetic nanostructures see Himpsel F J, Ortega J E, Mankey G J and Willis R F 1998 *Adv. Phys.* **47** 511
[20] Williams E D and Bartelt N C 1991 *Science* **251** 393
Viernow J, Lin J-L, Petrovykh D Y, Leibsle F M, Men F K and Himpsel F J 1998 *Appl. Phys. Lett.* **72** 948
Kirakosian A, Bennewitz R, Crain J N, Fauster Th, Lin J-L, Petrovykh D Y and Himpsel F J 2001 *Appl. Phys. Lett.* **79** at press
[21] Repain V, Berroir J M, Croset B, Rousset S, Garreau Y, Etgens V H and Lecoeur L 2000 *Phys. Rev. Lett.* **84** 5367
[22] Shapiro A P, Miller T and Chiang T-C 1988 *Phys. Rev.* B **38** 1779
Namba H, Nakanishi N, Yamaguchi T and Kuroda H 1993 *Phys. Rev. Lett.* **71** 4027
Ortega J E, Himpsel F J, Haight R and Peale D R 1994 *Phys. Rev.* B **49** 13 859
Wang X Y, Shen X J, Osgood R M, Haight R and Himpsel F J 1996 *Phys. Rev.* B **53** 15 738
Wang X Y, Shen X J and Osgood R M 1997 *Phys. Rev.* B **56** 7665
Baumberger F, Greber T and Osterwalder J 2000 *Phys. Rev.* B **62** 15 431
[23] Ortega J E, Speller S, Bachmann A R, Mascaraque A, Michel E G, Närmann A, Mugarza A, Rubio A and Himpsel F J 2000 *Phys. Rev. Lett.* **84**, 6110
[24] Avouris Ph and Lyo I-W 1994 *Science* **264** 942
Bürgi L, Jeandupeux O, Hirstein A, Brune H and Kern K 1998 *Phys. Rev. Lett.* **81** 5370
[25] Mugarza A, Pérez-Dieste V, Repain V, Rousset S, García de Abajo F J and Ortega J E 2001 *Phys. Rev. Lett.* at press

Ortega J E, Mugarza A, Pérez-Dieste V, Repain V, Rousset S and Mascaraque A to be published
[26] Jung T, Schlittler R, Gimzewski J K and Himpsel F J 1995 *Appl. Phys.* A **61** 467
Jung T, Mo Y W and Himpsel F J 1995 *Phys. Rev. Lett.* **74** 1641
Petrovykh D Y, Himpsel F J and Jung T 1998 *Surf. Sci.* **407** 189
[27] Gambardella P, Blanc M, Brune H, Kuhnke K and Kern K 2000 *Phys. Rev.* B **61** 2254
[28] Himpsel F J and Ortega J E 1994 *Phys. Rev.* B **50** 4992
[29] Pampuch C, Rader O, Kachel T, Gudat W, Carbone C, Klaesges R, Bihlmayer G, Blügel S and Eberhardt W 2000 *Phys. Rev. Lett.* **85** 2561
Dallmeyer A, Carbone C, Eberhardt W, Pampuch C, Rader O, Gudat W, Gambardella P and Kern K 2000 *Phys. Rev.* B **61** R5133
[30] Frank E R, Chen X X and Hamers R J 1995 *Surf. Sci.* **334** L709
Barth J V, Weckesser J, Cai C, Günter P, Bürgi L, Jeandupeux O and Kern K 2000 *Angew. Chem.* **112** 1285 (2000 *Int. Edn* **39** 1230)
[31] Bischler U and Bertel E 1993 *Phys. Rev. Lett.* **71** 2296
Bertel E and Lehmann L 1998 *Phys. Rev. Lett.* **80** 1497
For out-of-plane chains see Seki K, Karlsson U, Engelhardt R and Koch E E 1984 *Chem. Phys. Lett.* **103** 343
[32] Binns C and Norris C 1991 *J. Phys.: Condens. Matter* **3** 5425
[33] Pandey K C 1981 *Phys. Rev. Lett.* **47** 1913
Northrup J E, Hybertsen M S and Louie S G 1991 *Phys. Rev. Lett.* **66** 500
[34] Himpsel F J, Heimann P and Eastman D E 1981 *Phys. Rev.* B **24** 2003
Uhrberg R I G, Hansson G V, Nicholls J M and Flodstrom S A 1982 *Phys. Rev. Lett.* **48** 1032
Perfetti P, Nicholls J M and Reihl B 1987 *Phys. Rev.* B **36** 6160
See also Uhrberg R I G and LeLay G 2001 *J. Phys.: Condens. Matter* this special issue
[35] Whitman L J, Stroscio J A, Dragoset R A and Celotta R J 1991 *Phys. Rev. Lett.* **66** 1338
[36] Weitering H H, Chen J, DiNardo N J and Plummer E W 1993 *Phys. Rev.* B **48** 8119
Hebenstreit J, Heinemann M and Scheffler M 1991 *Phys. Rev. Lett.* **67** 1031
Hellberg C S and Erwin S C 1999 *Phys. Rev. Lett.* **83** 1003
[37] Erwin S C and Weitering H H 1998 *Phys. Rev. Lett.* **81** 2296 and references therein
[38] Yeom H W, Takeda S, Rotenberg E, Matsuda I, Horikoshi K, Schäfer J, Lee C M, Kevan S D, Ohta T, Nagao T and Hasegawa S 1999 *Phys. Rev. Lett.* **82** 4898
[39] Hill I G and McLean A B 1999 *Phys. Rev. Lett.* **82** 2155
[40] Pedreschi F, O'Mahony J D, Weightman P and Power J R 1998 *Appl. Phys. Lett.* **73** 2152
[41] Bauer E 1991 *Surf. Sci.* **250** L379
[42] O'Mahony J D, McGilp J F, Flipse C F J, Weightman P and Leibsle F M 1994 *Phys. Rev.* B **49** 2527
Shibata M, Sumita I and Nakajima M 1998 *Phys. Rev.* B **57** 1626
[43] Collins I R, Moran J T, Andrews P T, Cosso R, O'Mahony J D, McGilp J F and Margaritondo G 1995 *Surf. Sci.* **325** 45
Hill I G and McLean A B 1997 *Phys. Rev.* B **55** 15 664
[44] Losio R, Altmann K N and Himpsel F J 2000 *Phys. Rev. Lett.* **85** 808
[45] Jalochowski M, Strozak M and Zdyb R 1997 *Surf. Sci.* **375** 203
[46] Segovia P, Purdie D, Hengsberger M and Baer Y 1999 *Nature* **402** 504
[47] Losio R, Altmann K N, Kirakosian A, Lin J-L, Petrovykh D Y and Himpsel F J 2001 *Phys. Rev. Lett.* **86** 4632
[48] Altmann K N, Crain J N, Kirakosian A, Lin J-L, Petrovykh D Y, Himpsel F J and Losio R 2001 *Phys. Rev.* B **64** 035 406
Losio R, Altmann K N and Himpsel F J 2000 *Phys. Rev.* B **61** 10 845
[49] Sánchez-Portal D, Gale J D, García A and Martin R M 2001 *Preprint* cond-mat/0105400
[50] Erwin S C *et al* 2001 to be published
[51] Schäfer J, Rotenberg E and Kevan S D 2001 to be published
[52] Baski A A, Erwin S C, Turner M S, Jones K M, Dickinson J W and Carlisle J A 2001 *Surf. Sci.* **476** 22
[53] Yamada T, Bauschlicher C W and Partridge H 1999 *Phys. Rev.* B **59** 15 430
[54] Lipson H and Singer K E 1974 *J. Phys. C: Solid State Phys.* **7** 10
[55] Crommie M F, Lutz C P and Eigler D M 1993 *Science* **262** 218
Crommie M F, Lutz C P and Eigler D M 1993 *Nature* **363** 524
[56] Altmann K N, Bennewitz R, Crain J N, Kirakosian A, Lin J-L, McChesney J and Himpsel F J 2001 to be published
[57] Kevan S D 1995 *J. Electron Spectrosc. Relat. Phenom.* **75** 175
Mascaraque A, Avila J, Michel E G and Asensio M C 1998 *Phys. Rev.* B **57** 14 758
[58] Chulkov E V, Echenique P M, Liebsch A, Himpsel F J *et al* unpublished